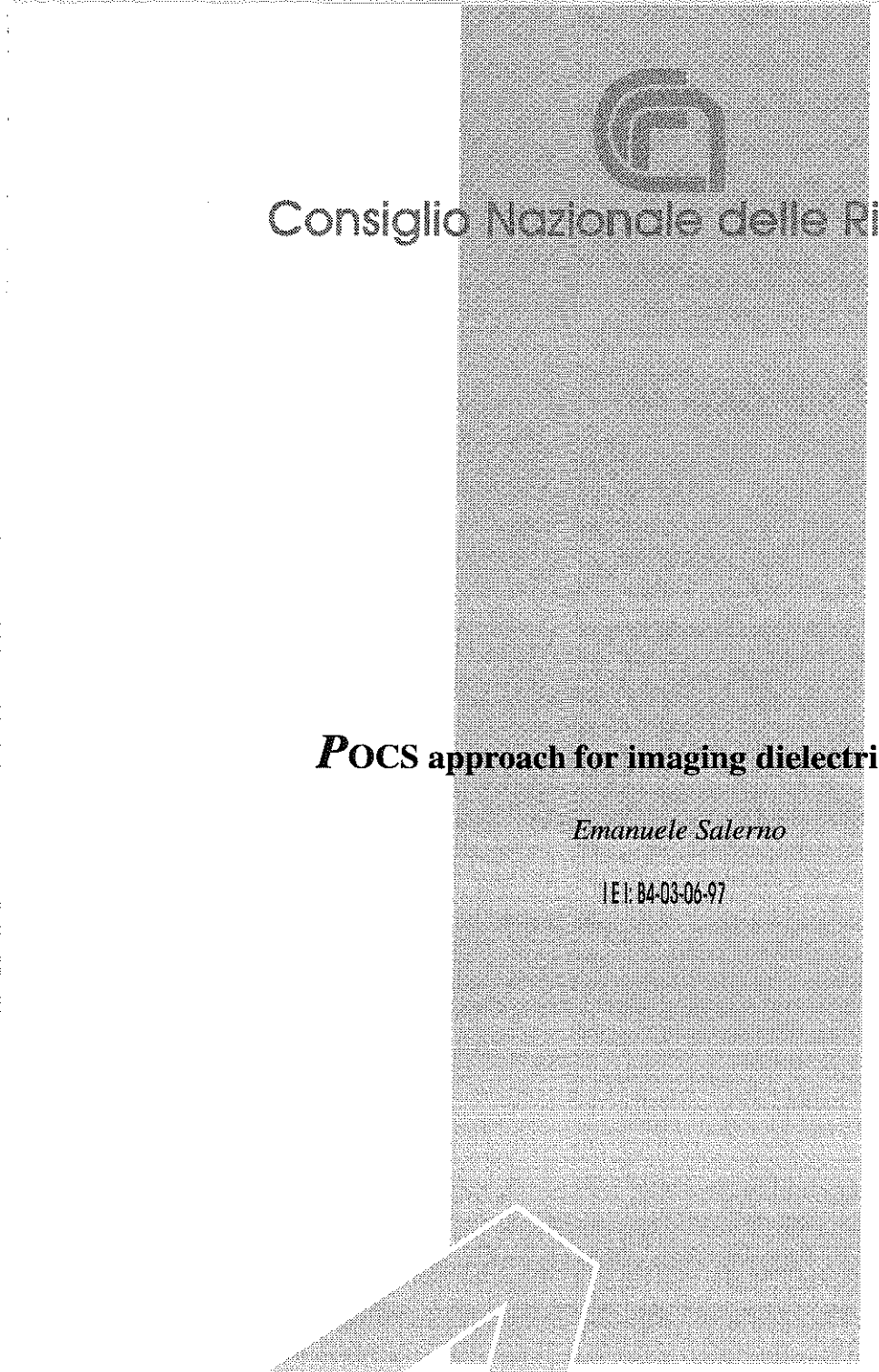

Consiglio Nazionale delle Ricerche

*P*OCS approach for imaging dielectric objects

Emanuele Salerno

I.E.I. B4-03-06-97

S.T.A.R.
Servizio Tecnografico Area di Ricerca del CNR - Pisa
responsabile della stampa Ermanno Scotti
maggio '97 134, 65

POCS Approach for Imaging Dielectric Objects [1]

Emanuele Salerno

Istituto di Elaborazione della Informazione - CNR

Via S. Maria, 46, I-56126 Pisa, Italy

Abstract

In this report, I consider the problem of reconstructing a tomographic image of a dielectric object from backscattering measurements. A data acquisition system coherently measures the electric field scattering at microwave frequencies, and a linear algorithm reconstructs a band-pass version of the object function. The first-order approximations usually adopted to linearize the inverse scattering problem greatly limit the possibility of imaging the object with sufficient fidelity. For objects with sensible contrast, the linear assumptions on the scattering equations are justified if the wavelength is similar to the size of the probed object. In many cases, the spatial resolution thus obtained is not satisfactory. In our case, furthermore, the passband does not contain the low-frequency part of the object function. A solution to these problems is to adopt fully nonlinear data models. This approach, however, normally leads to very costly algorithms. Another approach is to use a linear data model and a nonlinear reconstruction algorithm. An iterative Projection Onto Convex Sets (POCS) algorithm is proposed here, which exploits the measurement data, and additional information on the compact-support, the reality and the positivity of the solutions. This algorithm is studied both theoretically and experimentally, and its relationships with the Gerchberg method and the Projected Landweber method are pointed out.

Categories and Subject Descriptors: I.4.5 [**Image Processing**]: Reconstruction - *Transform methods*; J.2 [**Physical Sciences and Engineering**]: *Electronics*

1 Introduction

Microwave tomography applied to industrial nondestructive testing or evaluation is a promising technique, in that it offers certain advantages over other techniques [Bolomey, 1989, Bramanti and Salerno, 1992]. However, the scattering inversion implied in this technique is a difficult problem for the nonlinearity of the scattering equations, and algorithms based on fully nonlinear data models are normally very expensive (see for example [Garnero *et al.*, 1991, Caorsi *et al.*, 1993]). On the other hand, in the assumption of weak scattering, linear (Born or Rytov) approximations to the scattering equations can lead to linear reconstruction algorithms based on the inversion of a bandlimited portion of the object spectrum [Adams and Anderson, 1982, Baribaud *et al.*, 1985]. The weak scattering assumption for the Born approximation is valid when the wavelength is larger than the product between the average contrast and the diameter of the object under test [Slaney *et al.*, 1984]. If this condition is not satisfied, the data available are a distorted version of the object spectrum. Much work has been done in the past decades on linear scattering tomography; for some references, see [Bramanti and Salerno, 1992].
Another problem to be solved is the data acquisition system. Most of the tomographic systems that have been devised use plane-wave illumination and a multistatic measurement system. Several solutions have been proposed for its practical realization [Collignon *et al.*, 1982, Coté, 1992, Paoloni, 1987, Jacobi *et al.*, 1979, Bolomey and Pichot, 1990, Bolomey *et al.*, 1991, Caorsi *et al.*, 1991]. A very simple arrangement was proposed in [Mensa *et al.*, 1983], only considering far-field monostatic backscattering data. The illumination/measurement system is in this case very simple, and, in the linear assumptions, a very fast algorithm can be applied to re-

---

[1] Invited talk at the "Progress In Electromagnetics Research Symposium", PIERS'97, Cambridge, MA, July 7-11, 1997.

construct the image from band-pass 2D Fourier data. Unfortunately, the lack of the low-frequency region of the Fourier domain causes many ringing artifacts, which can completely mask the useful information in the reconstructed image. Besides the intrinsically low resolution imposed by the upper cutoff frequency of the imaging system, an additional problem thus arises from the presence of a lower cutoff frequency.
The requirements of a reliable data model and a simple hardware thus lead to the knowledge of the object spectrum over a rather narrow passband. An idea for recovering part of the missing spectrum, both at high and low spatial frequencies, could be to use a nonlinear reconstruction algorithm, exploiting the additional knowledge normally available. The underlying theory can be found in the literature on spectrum extrapolation and superresolution [Bertero and De Mol, 1996].
This report addresses the problem of tomographic reconstruction from the knowledge of a band-pass version of the object function, subject to compact-support, reality and positivity constraints. The object is assumed to be a real, non negative, square integrable function and the successive object estimates are considered as elements of the Hilbert space of the square integrable complex functions. A Projection Onto Convex Sets (POCS) algorithm is derived, which consists in cyclically projecting the image function orthogonally onto a number of closed convex sets; a fundamental theorem proves that this iteration converges to a function of their intersection, if it is nonempty. In our case, the compact-support constraint also assures convergence to the original object in the noiseless case. This algorithm is shown to be a generalization of the well-known Gerchberg superresolution algorithm [Gerchberg, 1974]. A further generalization, with the introduction of a relaxation parameter, shows that the algorithm can be seen as a version of the Projected Landweber method [Piana and Bertero, 1997]. The results are encouraging, in the sense that the obtained images are far better than the ones obtained by linear algorithms, and the computations are normally very fast if compared with the algorithms based on nonlinear data models.
In Section 2, I show the illumination and measurement system considered, and the linear data model obtained by using the first-order Born approximation. In Section 3, the reconstruction algorithm is described, with some hints on its convergence properties. Finally, in Section 4, the results of some simulated experiments are shown, along with the improvements obtained with respect to linear reconstruction and a rough evaluation of the computation times needed to reach the results. Some conclusions are drawn in Section 5.

2 A microwave backscattering tomographic system

Let us suppose having a system as in Figure 1, where a dielectric object is placed onto a rotating platform, and is illuminated by a plane-wave microwave radiation at frequency f, generated by a fixed antenna that also receives the backscattered field, which in its turn is coherently measured by the receiver. The object is a lossless dielectric, and is described by its 3D contrast function:

$$p(\boldsymbol{r}) = \frac{\varepsilon(\boldsymbol{r})}{\varepsilon_o} - 1 \quad , \tag{1}$$

where ε_o is the permittivity of the medium where the object is immersed, and $\varepsilon(\boldsymbol{r})$ is the (real) permittivity of the object, as a function of the 3D position vector $\boldsymbol{r} = (x,y,z)^T$, in a Cartesian coordinate system that rotates with the object. Let us consider the projection of the 3D contrast on the x-y plane:

$$g(x,y) = \int_{-\infty}^{\infty} p(x, y, z)\, dz \quad ; \tag{2}$$

we consider $g(x,y)$ as the object function to be reconstructed. Referring to the configuration shown in Figure 1, in the first-order Born approximation, if the receiving antenna is placed in

the far-field zone of the object, the complex envelope of the backscattered field will be given by (see [Bramanti and Salerno, 1992])

$$u_s(\theta) \approx -\frac{k^2}{4\pi} G\left(-\frac{2}{\lambda}\sin\theta, -\frac{2}{\lambda}\cos\theta\right) \frac{\exp\{jk\,d\}}{d} \quad , \tag{3}$$

where k is the wavenumber of the exploring radiation, λ is its wavelength, d is the distance of the phase center of the antenna from the rotation axis, and $G(f_x, f_y)$ is the 2D Fourier transform of our object function. It can be easily seen from (3) that for single frequency illumination the measured field can be directly related to the Fourier transform of the object function over a circumference with radius $2/\lambda$, centered in the origin of the Fourier plane. If multifrequency illumination is allowed, the object spectrum can be evaluated over an annulus, with inner and outer radii $2/\lambda_{max}$ and $2/\lambda_{min}$ if λ_{min} and λ_{max} are the minimum and maximum wavelength, respectively, of the exploring radiation.

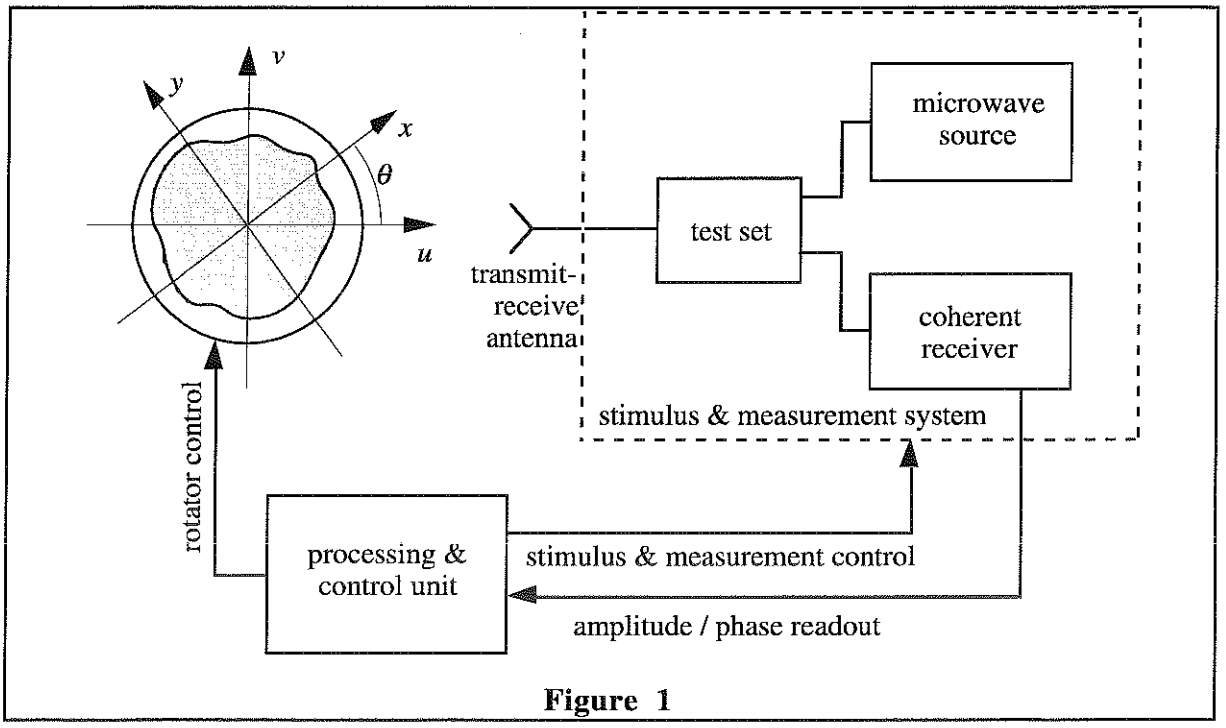

Figure 1

Assuming that the spectrum is zero outside the allowed annulus, a very fast reconstruction algorithm can be based on the interpolation of the data available over a Cartesian grid and an inverse fast Fourier transform. Another very fast approach is proposed in [Mensa *et al.*, 1983], which is based on a series of 1D fast circular convolutions, thus avoiding the 2D interpolation. The unfavorable shape of the system PSF in this case, however, causes the images to be extremely ambiguous. In [Mensa *et al.*, 1983], it is concluded that this technique is only suitable to image sparse arrays of pointform objects.

3 POCS approach to tomographic reconstruction

If the weak scattering assumption is satisfied, from the system described in the previous section, we obtain the values of the Fourier transform $G(f_x f_y)$ of the object function $g(x,y)$ over an annular domain B, with inner and outer radii $\rho_{min} = 2/\lambda_{max}$ and $\rho_{max} = 2/\lambda_{min}$, respectively. Let $g(x,y)$ be a real non-negative $L^2(\mathbb{R}^2)$ function with compact support X, contained in the compact region S (see Figure 2). The annular band-pass region B is described by the following $\mathbb{R}^2$ subset:

$$B = \left\{ (f_x, f_y) \in \mathbb{R}^2 \middle| \rho_{min} \le \sqrt{f_x^2 + f_y^2} \le \rho_{max} \right\} \quad . \tag{4}$$

It is to be noted that if G is identically zero outside B, then $g(x,y)$ cannot be a compact support function, apart from the trivial case of being zero everywhere [Herman and Tuy, 1987]. By the simple inverse transformation of the known part of G, one obtains the band-pass function $g_o(x,y)$. The band-pass version of a non-negative function is always severely distorted as it lacks the dc-component, which carries essential information for this type of image. However, we have additional information on the function to be reconstructed, and it can be used to extend the available part of the object spectrum. The information available on the problem leads us to formulate the requisites of our solution: we should find an $L^2(\mathbb{R}^2)$ function $g(x,y)$ such that:

$$FT^{-1}\{ G(f_x, f_y) \cdot I_B(f_x, f_y) \} = g_o(x, y) \tag{5 a}$$

$$\text{supp}\{ g(x, y) \} \in S \tag{5 b}$$

$$\Im\{ g(x, y) \} \equiv 0 \tag{5 c}$$

$$g(x, y) \ge 0 \tag{5 d}$$

where FT^{-1} denotes the inverse Fourier transform operator, supp{ } denotes the support of a function, $\Im\{g\}$ is the imaginary part of g, and $I_H(\alpha, \beta)$ denotes the characteristic function of the 2D domain H.

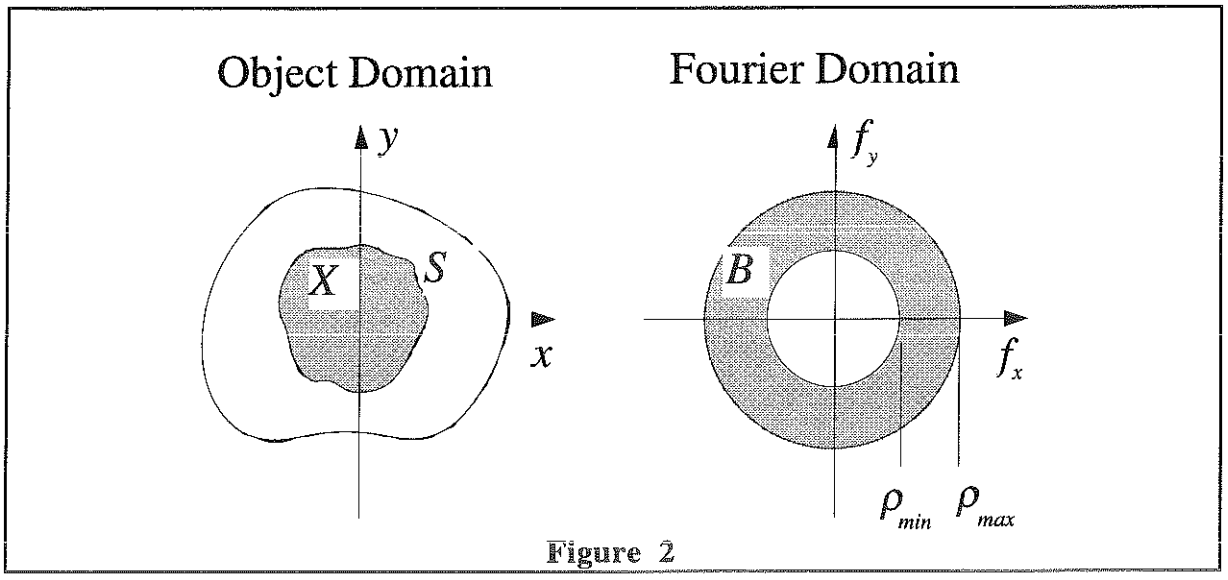

Figure 2

Let us now define the following subsets of $L^2(\mathbb{R}^2)$:

$$Q = \left\{ h(x,y) \in L^2(\mathbb{R}^2) \middle| \text{ supp}\{h\} \in S \right\} \tag{6 a}$$

$$R = \left\{ h(x,y) \in L^2(\mathbb{R}^2) \middle| \Im\{h(x,y)\} = 0, \ \forall (x,y) \in \mathbb{R}^2 \right\} \tag{6 b}$$

$$M = \left\{ h(x,y) \in L^2(\mathbb{R}^2) \middle| \Re\{h(x,y)\} \ge 0, \ \forall (x,y) \in \mathbb{R}^2 \right\} \tag{6 c}$$

$$D = \left\{ h(x,y) \in L^2(\mathbb{R}^2) \middle| FT\{h(x,y)\} \, I_B(f_x, f_y) = FT\{ g_o(x,y) \} \right\} \tag{6 d}$$

where FT is the Fourier transform operator, and $\Re\{h\}$ is the real part of h. A function $\hat{g}(x,y)$ satisfying (5) belongs to the intersection, A, of the sets (6 a-d):

$$A = Q \cap R \cap M \cap D \quad . \tag{7}$$

Observe that the intersection of the subsets D and Q contains a unique element. Indeed, each element of Q is a square integrable function with compact support and, by virtue of the Paley-Wiener theorem, its transform is an entire function. But if this element belongs to D as well, its transform will equal $FT\{g_o(x,y)\}$ in B. Being B a nonzero measure subset of the Fourier plane, only one such function exists, namely, $\hat{g}(x,y) = g(x,y)$. If the object function is real and nonnegative, then the set A defined in (7) contains one and only one element. We must find a procedure to evaluate this element.

It is easy to show that the subsets defined in (6) are closed and convex. Finding a function $\hat{g}(x,y)$ satisfying (5) is thus equivalent to finding an element of the intersection of a finite number of closed convex subsets of $L^2(\mathbb{R}^2)$. On the basis of a fundamental theorem [Herman and Tuy, 1987], we can state that, if we start from an arbitrary element of $L^2(\mathbb{R}^2)$ and cyclically project it orthogonally onto a finite number of closed and convex subsets, then we define a sequence converging to a point of their intersection. In our case, the sequence thus constructed converges to the unique element of A. We should only be able to derive explicit expressions for the orthogonal projections of a function onto the sets (6 a-d). Let us denote with $P_Z(h)$ the orthogonal projection of the function h on the subset Z, and consider, in turn, the subsets Q, R, M, and D:

a) The orthogonal projection of an $L^2(\mathbb{R}^2)$ function h onto the subset Q is:

$$P_Q(h) = I_S(x,y) \cdot h(x,y) \quad ; \tag{8}$$

b) The orthogonal projection of an $L^2(\mathbb{R}^2)$ function h onto R is

$$P_R(h) = \Re\{h\} \quad ; \tag{9}$$

c) The orthogonal projection of an $L^2(\mathbb{R}^2)$ function h onto M is

$$P_M(h) = \sup\{\Re\{h\}, 0\} + i\,\Im\{h\} \quad ; \tag{10}$$

d) The orthogonal projection of an $L^2(\mathbb{R}^2)$ function h onto D is:

$$P_D(h) = FT^{-1}\{FT\{h\}\,[1 - I_B(f_x, f_y)] + FT\{g_o\}\,I_B(f_x, f_y)\} \quad . \tag{11}$$

The proofs for Formulas (8)-(11) are reported in [Salerno, 1992a] and their derivation is similar to the one reported in [Herman and Tuy, 1987] for the case of limited-angle X-ray tomography (see also [Lent and Tuy, 1981]). Now, the algorithm to build the convergent sequence can be easily written down. Choose $g_o(x,y)$ as the iteration starting point, and let $\{g_j\}$ be the following sequence of functions (for $j = 0, 1, \ldots$):

projection on Q:

$$g_j'(x,y) = g_j(x,y)\, I_S(x,y) \tag{12 a}$$

projection on R:

$$g_j''(x,y) = \Re\left\{ g_j'(x,y) \right\} \tag{12 b}$$

projection on M:

$$g_j'''(x,y) = \sup\left\{ 0,\, g_j''(x,y) \right\} \tag{12 c}$$

projection on D:

$$g_{j+1} = \mathrm{FT}^{-1}\{[1 - I_B(f_x, f_y)]\ \mathrm{FT}\{g_j'''(x,y)\} + I_B(f_x,f_y)\mathrm{FT}\{g_o(x,y)\}\}. \quad (12\ \mathrm{d})$$

As mentioned above, the unique point of intersection between D and Q is $g(x,y)$. It follows that cyclical projections onto D and Q allow convergence to the same function of the complete scheme (12). The projections of the current estimate onto the subsets R and M thus introduce some amount of redundancy in the procedure; its effect is to speed up the convergence. The procedure obtained from steps (12 a) and (12 d) alone can be synthetically written as:

$$g_{j+1} = g_o + \mathrm{FT}^{-1}\{[1 - I_B]\ \mathrm{FT}\{g_j\ I_S\}\} \quad , \qquad (13)$$

and clearly coincides with the well-known Gerchberg algorithm [Gerchberg, 1974]. By suitably introducing a real parameter τ belonging to an appropriate interval, the iteration in (13) can be reduced to the Landweber method. In this case, by imposing nonlinear constraints (e.g., positivity, as in (12 c), the so-called Projected Landweber Method is obtained, which is normally faster than the non-projected method [Piana and Bertero, 1997]. This holds true for any allowed value of τ, and, in particular, for $\tau = 1$. Thus, our POCS procedure (12) can be seen as a particular version of the Projected Landweber method.
Note that our data model (3) does not consider the inevitable presence of the noise. When noise is present, the subset A does not contain a unique function anymore, indeed, it can also be unbounded. However, in this case the method shows a sort of semi-convergence property, in that the error in the solution first decreases, and then becomes increasing, with a velocity that depends on the signal-to-noise ratio [Piana and Bertero, 1997].
A theoretical study of the performance of the scheme (13) is reported in [Salerno, 1996], whereas a comparative theoretical-experimental study of the Gerchberg and the Projected Landweber schemes is now being performed. The algorithm (12) has been already experimented on real backscattering measurements, from the system shown in the previous section [Bramanti and Salerno, 1992, Salerno, 1992a, 1992b]. Numerical experiments are now being performed using a synthetic phantom, in order to evaluate the performance of the method. Part of the results of this analysis are reported in next section.

4 Experimental results

The tests reported in this section are intended to analyze the performance of the proposed algorithm both in the noiseless and the noisy cases. By using only simulated data, we can control the noise level and we can also assume some quantitative index to evaluate the performance.
The synthetic phantom adopted for the experiments is shown schematically in Figure 3. The magnitude of its Fourier transform is shown in Figure 4; the grayscale used is linear (white = minimum, black = maximum). The represented domain in the f_x-f_y plane is the square region [-8, 8]×[–8, 8], discretized in a 256×256 grid. For all the experiments, the inner and outer radii of the passband, respectively, have been set to $\rho_{min} = 1$ and $\rho_{max} = 2$. The object support is assumed to be the circle with center in (0,0) and radius 1.5. The magnitude of the initial data function $I_B(f_x f_y)G(f_x f_y)$ is shown in Figure 5. Its inverse transform is shown in Fig. 6.
As can be seen, the result of this direct inversion is very unsatisfactory, in that the artifact level is often higher than the level of the useful signal. The experiments shown here prove that, by using procedure (12), the reconstructed image is greatly improved, with a reasonable computational cost. Indeed, the non optimized test code, in any case, took a few minutes on an Hp9000/720 workstation, including some interactive input/output operation and the disk storage of the current estimate at each iteration.

4.1 Noiseless case

For the noiseless experiments, the image in Figure 6 was assumed as our g_o. A typical result obtained by the proposed algorithm is shown in Figure 7. The magnitude of the related spectrum is shown in Figure 8. In this case, 164 iterations of procedure (12) were applied. We can immediately note that a significant extension of the spectrum has been achieved, both in the high frequency and the low frequency regions of the Fourier plane, and this permitted a significant reduction in the oscillating artifacts affecting Figure 5. It is interesting to note that a visually very similar result is obtained both for 10 and for 2000 iterations. This means that the

convergence of the POCS scheme is very fast for the first few iterations, and becomes very slow afterwards, but the "cosmetic" quality of the solution does not increase significantly after a reasonable number of iterations. We assumed the rms error between the solution and the original in Figure 1 as a quality index for the solution. In Figure 9, a plot of the rms error as a function of the iteration number is shown, compared with the corresponding result of the Gerchberg scheme (13). As can be clearly seen, the use of the positivity and reality constraints makes the convergence much faster.

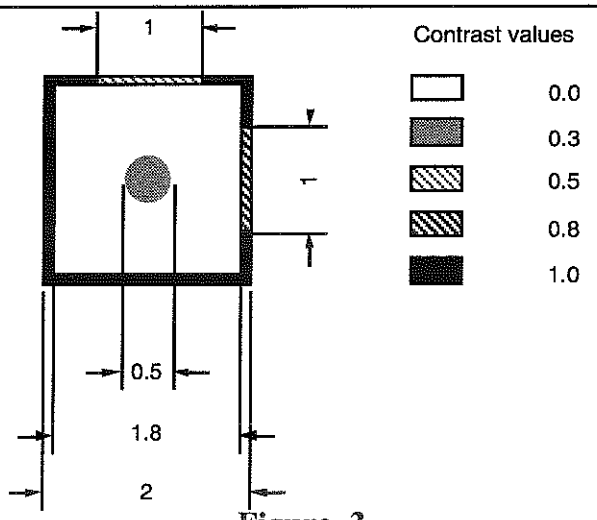

Figure 3

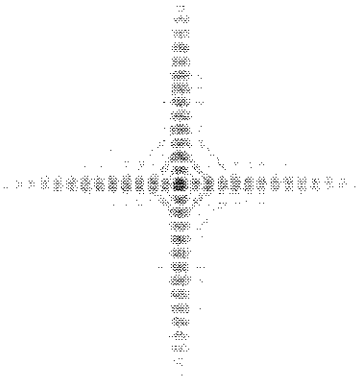

Figure 4

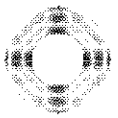

Figure 5

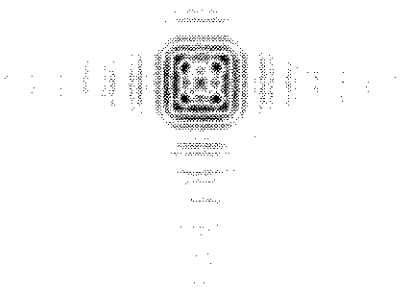

Figure 6

Figure 7

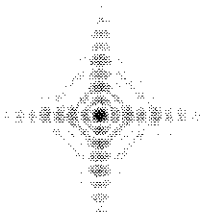

Figure 8

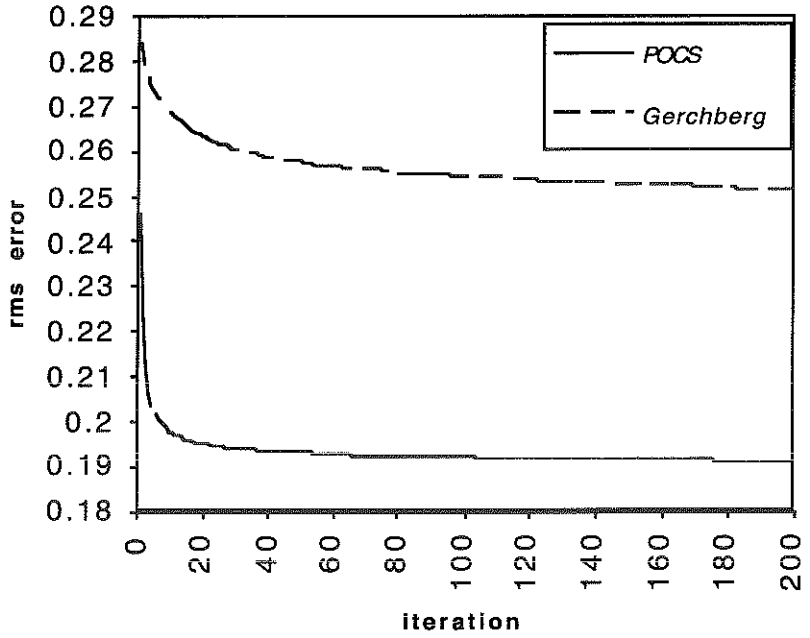

Figure 9

4.2 Noisy cases

The noisy cases were produced by adding different amounts of Gaussian white noise to the Fourier data shown in Figure 4.

The algorithm proposed here turned out to be very robust against noise. As an example, in Figures 10 and 11, we show the results obtained with a noise standard deviation $\sigma = 0.1$ (corresponding to an SNR of about 0.13 dB). Figure 10 shows the solution after 100 iterations, Figure 11 shows its spectrum. In this case, the degradation with respect to the noiseless case is evident; in other cases it can be only derived from the error values.

In Figure 12, the rms errors for the first 100 iterations are plotted, for different values of the noise standard deviation. This figure illustrates the above-mentioned semi-convergence property of the method. The minimum rms error is reached at an iteration number that increases with decreasing noise, and its value decreases with the noise. For $\sigma = 0.02$ (SNR $\approx$ 14 dB), the minimum is not reached within the displayed iteration range. In the limit for σ approaching zero (i.e., in the noiseless case), the minimum is obviously zero and is reached at infinity.

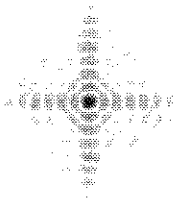

Figure 10 **Figure 11**

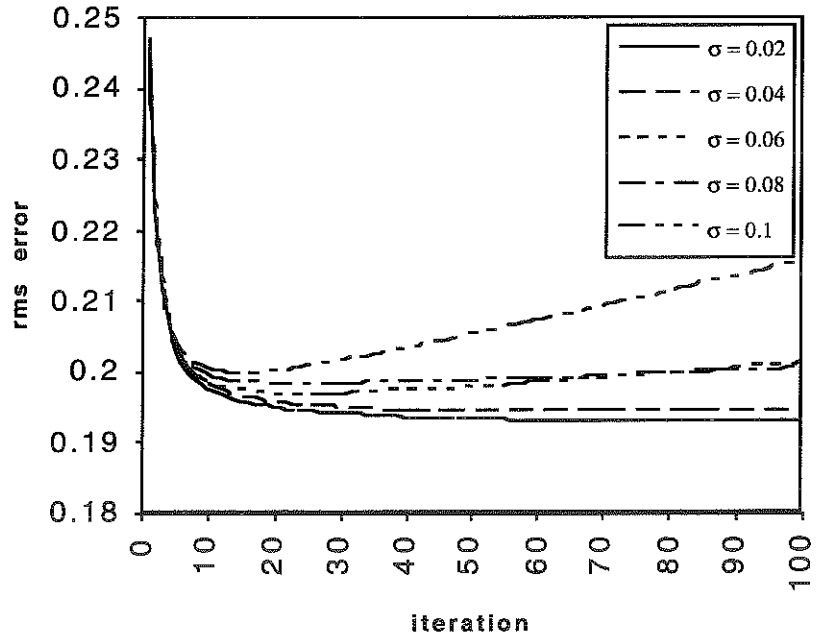

Figure 12

5 Discussion and conclusions

As mentioned above, the first-order Born approximation is justified only if the incident radiation is weakly scattered by the object, and this happens when the contrast multiplied by the object size is conveniently smaller than the wavelength of the probing radiation. If this is true, the measured field is related as shown in (3) to the Fourier transform of the contrast function. Otherwise, the initial data will be a somewhat distorted version of the passband portion of the transform.

The spatial resolution attainable by Fourier inversion of the available data is of the order of half a wavelength (see [Bramanti *et al.*, 1986]). This means that the wavelength should be reduced as much as possible, but this approach has its limits, because any physical body is less and less transparent to electromagnetic radiation with decreasing wavelengths, and the resulting distortion would become unacceptable. A solution to this problem could be the fully nonlinear solution of the scattering equations. Another approach, as I suggest here, could be to tune the radiation wavelength to meet the Born requirements, or to allow some reduced distortion, and then adopt a spectrum extrapolation algorithm to recover part of the missing object spectrum.

For typical situations, the possibilities of the algorithm described here are certainly significant, both in terms of resolution and artifact suppression. Owing to the slow convergence after the

first few iterations, the practical resolution limits attainable are not unlimited, even for very favorable SNRs. Note also that, for strongly mismatched objects, Equation (3) holds true only if the minimum wavelength is much larger than the object size. This means that, although the wavelength is not an ultimate limitation, the resolution achievable may be unsatisfactory for many applications. Thus, this algorithm cannot be strictly considered as a good candidate for true quantitative microwave imaging: a feature that is often claimed for algorithms based on fully nonlinear data models. However, it has the advantage of being not very computationally expensive, and yields much better images than any linear reconstruction algorithm.
The algorithm described in this paper was designed specifically for band-pass data, and has been shown to be very efficient in this particular case. Nevertheless, it could be applied to initial data belonging to any dense subset of the Fourier plane, such as the one obtained from limited-angle backscattering measurements. We plan to consider this aspect of the problem in the future.

References

Adams, M.F., Anderson, A.P., 1982, "Synthetic Aperture Tomographic (SAT) Imaging for Microwave Diagnostics", IEE Proc., Vol. 129, pt. H, No. 2, pp. 83-88.

Baribaud, M., Dubois, F., Floyrac, R., Wang, S., 1985, "Tomographic Image Reconstitution of Objects from Multi-incidence Microwave Exploration", *IEE Proc.*, Vol. 132, pt. H, No. 5, pp. 286-290.

Bertero, M., De Mol, C., 1996, "Super-Resolution by Data Inversion", in E. Wolf Ed., *Progress in Optics*, Vol. XXXVI, North Holland.

Bolomey, J.C., 1989, "Recent European Developments in Active Microwave Imaging for Industrial, Scientific, and Medical Applications", *IEEE Trans.*, Vol. MTT-37, No. 12, pp. 2109-2117.

Bolomey, J.C. Pichot, C., 1990, "Microwave Tomography: From Theory to Practical Imaging Systems", *Int. J. of Imag. Syst. and Technology*, Vol. 2, pp. 144-156.

Bolomey, J.C., Pichot, C., Gaboriaud, G., 1991, "Planar Microwave Imaging Camera for Biomedical Applications: Critical and Prospective Analysis of Reconstruction Algorithms", *Radio Science*, Vol. 26, No. 2, pp. 541-549.

Bramanti, M., Tonazzini, A., Salerno, E.A., 1986, "Some Theoretical Aspects of a Backscattering Based Tomographic Imaging Technique", *Signal Processing*, Vol. 10, No. 4, pp. 415-425.

Bramanti, M., Salerno, E., 1992, "Electromagnetic Techniques for Nondestructive Testing of Dielectric Materials: Diffraction Tomography", *J. of Microwave Power and Electromagnetic Energy*, Vol. 27, No. 4, pp. 233-240.

Caorsi, S. Gragnani, G.L. Pastorino, M., 1991, "A Multiview Microwave Imaging System for Two-Dimensional Penetrable Objects", *IEEE Trans.*, Vol. MTT-39, No. 5, pp. 845-851.

Caorsi, S., Gragnani, G.L., Pastorino, M., 1993, "Reconstruction of Dielectric Permittivity Distributions in Arbitrary 2-D Inhomogeneous Biological Bodies by a Multiview Microwave Numerical Method", *IEEE Trans.*, Vol. MI-12, No. 2, pp. 232-239.

Collignon, G., Michel, Y., Robin, F., Saint, J., Bolomey, J.C., 1982, "Quick Microwave Field Mapping for Large Antennas", *Microwave Journal*, pp. 129-132.

Coté, M.G., 1992, "Automated Swept-Angle Bistatic Scattering Measurements Using Continuous Wave Radar", *IEEE Trans. on Instr. & Meas.*, Vol. IM-41, No. 2, pp. 185-192.

Garnero, L., Franchois, A., Hugonin, J.-P., Pichot, C., Joachimowicz, N., 1991, "Microwave Imaging - Complex Permittivity Reconstruction by Simulated Annealing", *IEEE Trans.*, Vol. MTT-39, No. 11, pp. 1801-1807.

Gerchberg, R.W., 1974, "Super-resolution through Error-Energy Reduction", *Optica Acta*, Vol. 21, No. 9, pp. 709-720.

Herman, G.T., Tuy, H.K., 1987, "Image Reconstruction from Projections: An Approach from Mathematical Analysis", in P.C. Sabatier (ed.), *Basic Methods of Tomography and Inverse Problems*, Adam Hilger, Bristol and Philadelphia.

Jacobi, J.H. Larsen, L.E. Hast, C.T., 1979, "Water-Immersed Microwave Antennas and their Application to Microwave Interrogation of Biological Targets", *IEEE Trans.*, Vol. MTT-27, pp. 70 - 78.

Lent, A., Tuy, H.K., 1981, "An Iterative Method for the Extrapolation of Band-limited Functions", *J. Math. Anal. and Appl.*, Vol. 83, pp. 554-565.

Mensa, D., Halevy, S., Wade, G., 1983, "Coherent Doppler Tomography for Microwave Imaging", *IEEE Proc.*, Vol. 71, No. 2, pp. 254-261.

Paoloni, F.J., 1987, "Implementation of Microwave Diffraction Tomography for Measurement of Dielectric Constant Distribution", *IEE Proc.*, Vol. 134, Pt. H, No. 1, pp. 25-29.

Piana, M., Bertero, M., 1997, "Projected Landweber Method and Preconditioning", *Inverse Problems*, Vol. 13, No. 2, pp. 441-463.

Salerno, E.A., 1992a, "The Gerchberg and POCS Approaches in Spectrum Extrapolation of Band-Pass Tomographic Images", IEI-CNR, Pisa, N.I. B4-01-92.

Salerno, E.A., 1992b, "Achieving Super-Resolution with Band-Pass Images", in *Signal Processing VI: Theories and Applications*, J. Vandewalle *et al.*, editors, Elsevier, pp. 1417-1420.

Salerno, E.A., 1996, "Eigenvalue Analysis of an Iterative Super-Resolution Operator for 2D Band-Pass Images", *Proc. SIMAI '96*, Salice Terme, Italy, 27-31/5/1996, SIMAI, pp. 518-520.

Slaney, M., Kak, A.C., Larsen, L.E., 1984, "Limitations of Imaging with First Order Diffraction Tomography", *IEEE Trans.*, Vol. MTT-32, No. 8, pp. 860-874.